Proceedings of ICFDP 8:
Eight International Congress of Fluid Dynamics & Propulsion
Sharm El-Shiekh, Sinai , Egypt, Dec. 14 -17, 2006

ICFDP8-EG-169

Numerical Simulation of Air Humidification Process in a Duct Using a Multi-Sprays System

Samy M. Morcos
Professor of Fluid Mechanics, Cairo University, Egypt

Mahmoud A. Fouad
Professor of Fluid Mechanics, Cairo University, Egypt

Hafez A. El-Salmawy
Associate Professor, Department of Mechanical Power Engineering, Zagazig University, Egypt

Kareem M. Awny
Teaching Assistant, Department of Mechanical Power Engineering, Cairo University, Egypt

ABSTRACT

A three dimensional numerical model has been developed to simulate humidification process resulting from a matrix of sprays placed at the entrance of a rectangular duct. The model considers full coupling between the sprays and the turbulent airflow. A stochastic treatment has been utilized for the turbulence, liquid injection and collisions between droplets. The simulation is based on the open source code KIVA-III. This enabled some modeling, adaptation and solution algorithm modifications to the original code. These include modifications to the droplets collision model, use of an efficient consecutive numerical blocks solution algorithm and simulation of interactions between sprays as well as duct boundaries. The results showed the dependency of the humidification efficiency on the droplets dispersion, especially at the first part after the injection plane. The cross-flow injection is the most efficient orientation regarding humidification efficiency, while the counter flow injection offers the best final sectional homogeneity. The decrease in the injected Sauter mean diameter improves the humidification efficiency. The inlet air turbulent kinetic energy has a minor effect on the humidification process due to its rapid decay.

INTRODUCTION

Humidity control is an important parameter in many fields. It has a noticeable impact on human health and comfort as well as productivity. In industry, improper humidity control can cause damage to many kinds of equipment and materials. This can be noticed in industries such as: textile, paper and electronic chips. Recently use of inlet duct cooling of gas turbine utilizing an evaporative cooling system at the inlet duct has been in focus [1]. This is due to its advantages not only in recovering power loss due to the change in the ambient conditions but also augmenting the gas turbine output as well as efficiency.

Evaporative cooling can be achieved by spraying water into the air or passing the air through a wetted packed material. The later technique suffers from air pressure loss. This gives the humidification by atomization an advantage. Humidification by atomization can be achieved using a matrix of atomizers installed in the inlet of the humidification section. Water injected from the atomizers disintegrates into droplets that flow with the air stream forming an evaporating two phase flow.

Evaporative spray humidification can be classified as liquid atomization and two phase flow with phase change. To predict the performance of spray humidification system, phenomena such as liquid atomization, spray/airflow interaction and droplet evaporation should be well understood. Also several parameters can affect the system performance such as spray/airflow orientation, interaction between sprays, in case of relying on more the one spray, and effect of the flow field characteristics on spray behavior as well as evaporation.

Several researchers had studied these phenomena either from fundamental or application perspectives. Injection of a spray into the cross-flow has been studied by Ghosh and Hunt [2]. Their main goal was to develop an analytical solution describing the trajectory of the various spray size classes, as shown in Fig.1. The analysis assumed spherical droplets. They neglected droplet collision, secondary breakup, and vaporization effects. Depending on the magnitude of the cross-flow velocity, the modeled spray was comprised of different zones. For example, in case of weak cross-flow velocities (U_{cross} /U_{jet} <0.1), the zones comprising the spray include three zones A, B and C. At zone (A) the induced vertical air velocity within the spray entrains the surrounding air into the spray leading to an increase in the spray volume. At zone (B) the

surrounding air is still entrained into the jet while small droplets are being dispersed downstream. At zone (C), small droplets are still being dispersed while the cross-airflow passes through the spray is not able to divert the large droplets. For moderate cross-flow velocities (U_{cross} /U_{jet} >0.3), zone (A) will not be presented and the spray consists of zones (B) and (C) as described above. In this case new zone is added which is zone (D). In this zone, the cross-flow passes through the spray is able to disperse large droplets.

Mashayek et al. [3] used direct numerical simulations to simulate droplet dispersion in an isotropic turbulent flow. The evaporation is governed by the classical "D^2 law" and the mass loading was small enough to neglect turbulence modulation by the dispersed phase (one-way coupling). More recently, Mashayek, [4] removed this restriction and considered droplet dispersion in compressible homogeneous turbulent flow with two-way coupling.

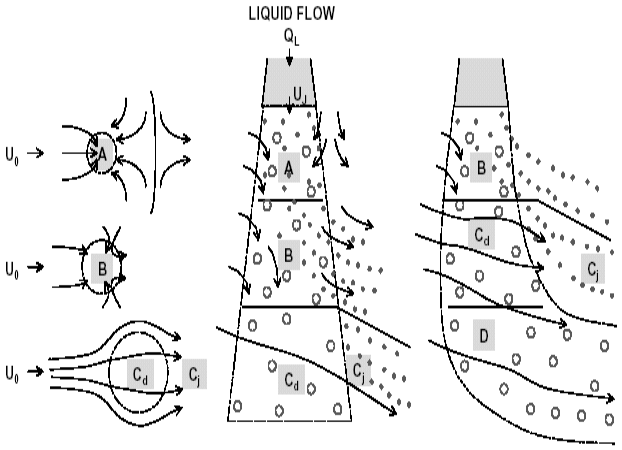

Fig. 1 Zones used to analyze the trajectory of the spray jet in cross-flow. [1]

As a part of the validation process of their model, Crowe et al.[5] demonstrated the application of their "Particle-Source-In Cell" (PSI-CELL) model in a spray cooling system. The system consisted of jets of water sprays injected at an angle into a cross-flow for air cooling. The model predicted the trajectories of specified droplet sizes, as well as the gas flow field. Other than demonstrating the model on this type of flow, this study did not include any parametric variation on the system. Kachhwaha et al [6] performed an experimental and numerical study for evaporative cooling of air by water spray. The developed model is a two-dimensional which uses the maximum entropy principle (MEP) to determine the injected droplet distribution probability function. The experimental tests and the numerical simulations were performed for horizontal parallel flow. Kachhwaha et al [7] used the same model to simulate horizontal counter flow water spray. No parametric study was performed in this work, but the result showed less accuracy in the prediction of the counter flow spray.

Sanjeev Jolly et al. [8] studied experimentally the performance of a system for evaporative cooling using high-pressure water spray installed at the inlet of the intake duct of a gas turbine unit. The system consisted of an array of nozzles distributed uniformly on the cross section of the inlet duct. The results showed that, it is important to limit the size of the water droplets in order to allow for vaporization of water in a relatively short distance. Also injection of the spray at a low air velocity is preferable to increase the traveling time of the droplets.

The present work presents a three dimensional numerical simulation for the humidification process of an ambient air stream flows in a rectangular duct using two dimensional matrix of uniformly arranged water spraying nozzles. The model accounts for the effects of sprays interactions, droplet breakup, evaporation and collision. The developed solution is used to perform a parametric study to evaluate the impact of some operational and design parameters on humidification efficiency and homogeneity.

DESCRIPTION OF THE PHYSICAL MODEL

The considered physical model simulates a matrix of water spray nozzles located at the inlet of a humidification section simulating an air handling unit or inlet duct of a gas turbine. The injection matrix is shown in Fig. 2. The humidification section has a constant cross section. The injection matrix consists of a set of parallel feeders. The nozzles are arranged along each feeder, such that, injection is in the direction perpendicular to the feeder axis. The nozzles are installed on the feeder in pairs; each pair consists of a nozzle facing up and the other facing down. The distance between two consecutive pairs is constant, as shown in Fig. 2.

NOMENCLATURE

a	pressure gradient scaling parameter
B_d	Droplet transfer number
C_D	Drag coefficient (N)
$C\mu$	Coefficient in turbulence model
c_l	The liquid specific heat (kJ/kg.K)
C_P	The specific heat of the carrier phase at constant pressure (kJ/kg.K)
D	Mass diffusion coefficient (m^2/s)
D, d	Diameter (m)
I	Specific internal energy (J/kg)
k	Kinetic energy of turbulence (J/kg)
k_{air}	Thermal conductivity (W/m.K)
L	Latent heat of vaporization (J/kg),

l	Length scale (m)
M, m	Mass (kg)
$\dot{m}$	Mass flow rate (kg/s)
P	Mean pressure (Pa)
r	Droplet radius (m)
R	Rate of droplet radius change
r_{32}	Sauter mean droplet radius (m)
Re_d	Reynolds number
R.H.	Air relative humidity
SMD	Sauter mean diameter ($\sum D^3 / \sum D^2$) (m
St. dev.	Standard deviation
T	Gas temperature (K)
TKE	Turbulent kinetic energy (m^2/s^2)
t	Time (second)
$\bar{u}$	Mean velocity (m/s)
$\vec{u}'$	The Gas turbulence velocity (m/s)
W_i	The molecular weight (kg/kmol)

Greek Symbols:

μ	Dynamic viscosity (kg/m.s)
ρ	Density (kg/m^3)
ε	The Rate of turbulence energy dissipation (J/kg.s)
ν	Collision frequency
ψ	Absolute humidity

Subscripts:

av.	Average value
db	Dry bulb temperature
g	Gas
f	Fluid
in	Inlet condition
l	Liquid
o	Initial
p	Particule

MODEL GOVERNING EQUATIONS

The governing equations for both the carrier and dispersed phases are as follows:

Continuity Equation

The continuity equation of gaseous species m is

$$\frac{\partial \rho_m}{\partial t} + \nabla \cdot [\rho_m \vec{u}] = \nabla \cdot \left[\rho D \nabla \left(\frac{\rho_m}{\rho} \right) \right] + \dot{\rho}^S \delta_{m1} \quad (1)$$

Where $\dot{\rho}^S$ is the source term of the spray, it takes the following form.

$$\dot{\rho}^S = -\int f \rho_d \, 4\pi r^2 R d\vec{v} dr dT_d dy d\, y \quad (2)$$

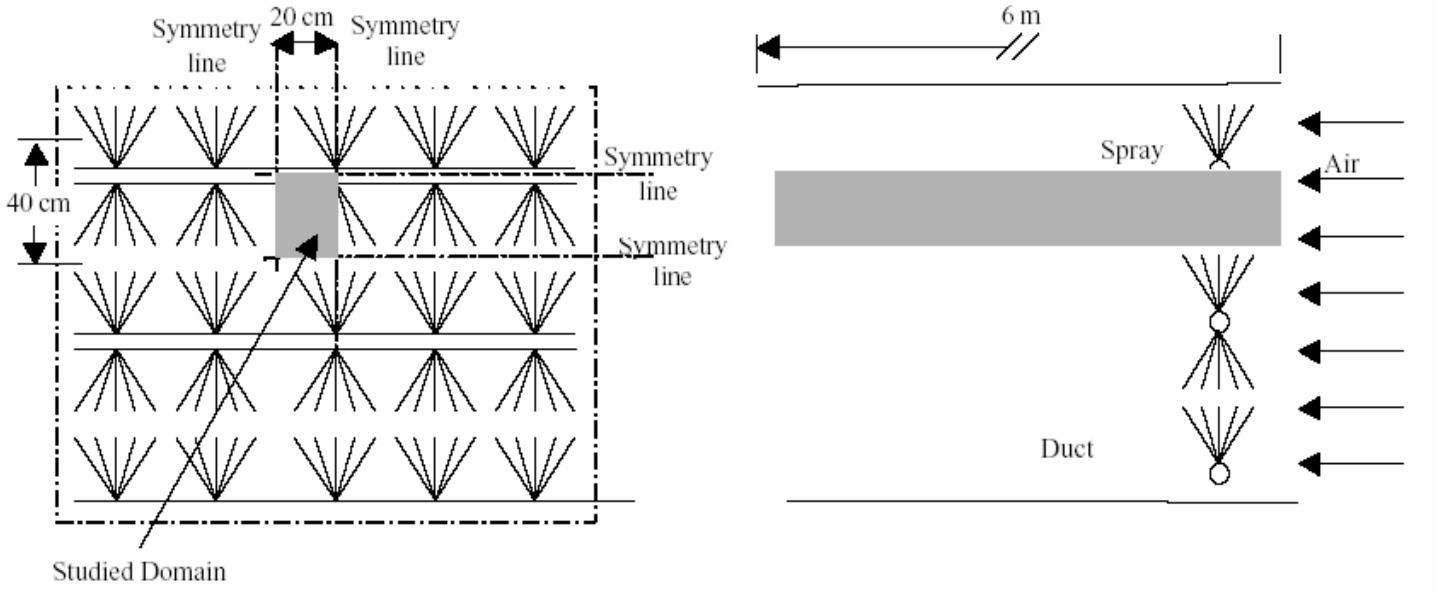

Fig.2 The Physical Model

Momentum Equation

The momentum equation for the fluid mixture is

$$\frac{\partial \rho \vec{u}}{\partial t} + \nabla \cdot [\rho \vec{u}\vec{u}] = -\frac{1}{a^2} \nabla p - \nabla \left(\frac{2}{3} \rho k \right) + \nabla \cdot \sigma + F^s + \rho g \quad (3)$$

Where "a" is the dimensionless quantity used in conjunction with pressure gradient scaling (PGS) method to improved solution stability and accuracy [9]. F^s is the rate of momentum gain per unit volume due to spray, which has the following form.

$$\vec{F}^S = -\int f \rho_d \left(\frac{4}{3} \pi r^3 \vec{F} + 4\pi r^2 R \vec{v} \right) d\vec{v} dr dT_d dy d\, y \quad (4)$$

Energy Equation

The internal energy equation is as follows.

$$\frac{\partial \rho I}{\partial t} + \nabla \cdot \left[\rho \, \vec{u} I\right] = -p\nabla \cdot \vec{u} - \nabla \cdot J + \rho\varepsilon + Q^s \quad (5)$$

The heat flux vector J is the sum of heat conduction and enthalpy diffusion.

$$J = -k\nabla T - \rho D \sum_m h_m \nabla \left(\frac{\rho_m}{\rho}\right) \quad (6)$$

Q^s is the source term of the spray in the energy equation.

$$\dot{Q}^S = -\int f\rho_d \left\{(4\pi r^2 R\left(I_l(T_d) + \frac{1}{2}(\vec{v} - \vec{u})^2\right) + \frac{4}{3}\pi r^3\left(C_l T_d + \vec{F} \bullet (\vec{v} - \vec{u} - \vec{u}')\right)\right\} d\vec{v} dr dT_d dy d y \quad (7)$$

Where $I_l(T_d)$ is the internal energy of the liquid phase.

Turbulence model equations

In order to consider the effect of the local eddy size on the turbulence as well as to minimize the effect of the computational grid on the accuracy of the turbulence prediction, a technique which switches between a modified k-Є model and Sub-Grid Scale model (SGS) has been adopted. The switching is carried out according to the local eddy size. In the SGS model only the turbulent kinetic energy equation is considered while its dissipation is defined according to the local eddy size. The k-Є model has been modified to take into account the presence of the droplets in the gas and their effect on turbulence destruction. The equations of the modified k-Є are as follows.

$$\frac{\partial \rho k}{\partial t} + \nabla \cdot \left[\rho_m \vec{u} k\right] = -\tfrac{2}{3}\rho k \nabla \vec{u} + \tau : \nabla u + \nabla \cdot \left[\left(\frac{\mu}{\mathrm{Pr}_k}\right)\nabla k\right] - \rho\varepsilon + \dot{W}^s \quad (8)$$

$$\frac{\partial \rho\varepsilon}{\partial t} + \nabla \cdot \left[\rho \, \vec{u}\varepsilon\right] = -\left(\tfrac{2}{3}c_{\varepsilon_1} - c_{\varepsilon_3}\right)\rho\varepsilon\nabla\vec{u} + \nabla \cdot \left[\left(\frac{\mu}{\mathrm{Pr}_\varepsilon}\right)\nabla\varepsilon\right] + \frac{\varepsilon}{k}\left[c_{\varepsilon_1}\tau : \nabla\vec{u} - c_{\varepsilon_2}\rho\varepsilon + c_s W^s\right] \quad (9)$$

Where W^S is the source term arises due to the interaction with the spray, it can be defined as follows.

$$\dot{W}^S = -\int f\rho_d \left(\frac{4}{3}\pi r^3 \vec{F} u'\right) d\vec{v} dr dT_d dy d y \quad (10)$$

$\dot{W}^S$ is the negative of the rate at which turbulent eddies are doing work in dispersing the spray droplets. Since u' follows the Gaussian distribution it can be shown that $\dot{W}^S < 0$. This term is responsible for turbulent depletion due to droplets existence.

The quantities $c_{\varepsilon_1}, c_{\varepsilon_2}, c_{\varepsilon_2}, p_{rk}, and \quad p_{r\varepsilon}$ are constants whose values are determined from experiments and some theoretical considerations [9]. The values of these constants are given in the table 1.

Table 1 Values of modified k-Є turbulence model constants

$c_{\varepsilon 1}$	$c_{\varepsilon 2}$	$c_{\varepsilon 3}$	$p_{r\varepsilon}$	p_{rk}
1.44	1.92	-1.0	1.3	1.0

Switching between the SGS model and the k-Є model depends on the eddy size compared with the local computational grid size. If the eddy size predicted by the k-□ model is larger than a pre-assigned length scale, which depends on the grid size, the SGS model is used to predict the turbulence. This constrain takes the following form:

$$\varepsilon \geq \left[\frac{c_\mu}{P_{r_\varepsilon}\left(c_{\varepsilon_2} - c_{\varepsilon_1}\right)}\right]^{1/2} \frac{k^{3/2}}{L_{SGS}} \quad (11)$$

Where L_{SGS} is the pre-assigned length scale and it is taken to be 4 δx, where δx is a representative computational cell dimension. The eddy size is taken to be proportional to $k^{3/2}/Є$.

Droplet Momentum Equation

The droplet momentum equation along its trajectory is as follow

$$\frac{d\vec{u}_p}{dt} = \frac{3}{8}\frac{\rho}{\rho_d}\frac{\left|\bar{u} + u' - \bar{u}_p\right|}{r}\left(\bar{u} + u' - \bar{u}_p\right)C_D \quad (12)$$

The drag coefficient C_D is given by

$$C_D = \begin{cases} \dfrac{24}{\mathrm{Re}_d}\left(1 + 1/6\,\mathrm{Re}_d^{2/3}\right) & R_{ed} < 1000 \\ 0.424 & R_{ed} > 1000 \end{cases} \quad (13)$$

Where

$$\mathrm{Re}_d = \frac{2\rho\left|\bar{u} + u' - \bar{u}_p\right| r_p}{\mu_{air}(\hat{T})}, \quad (14)$$

$$\hat{T} = \frac{T + 2T_d}{3}, \quad (15)$$

The gas turbulence velocity u' is added to the local mean gas velocity when calculating the droplet's drag. It is assumed that each component u' follows a Gaussian distribution with a mean square deviation 2/3k [9].

Auxiliary Equations

The working fluid is taken as a perfect gas. Relations for gases mixture are considered to calculate the gas properties. Regarding the transport coefficients they are considered as follows:

For viscosity

$$\mu = \mu_{air} + C_\mu \, k^2/\varepsilon \tag{16}$$

Where C_μ is an empirical constant with a standard value of 0.09 [9]. And μ_{air} can be calculated according to the following relation [9]:

$$\mu_{air} = \frac{A_1 T^{3/2}}{T + A_2} \tag{17}$$

Where A_1 and A_2 are constants, their values are 1.458×10^{-6} kg/(m s $K^{0.5}$) and 110.4 K respectively [9]. Thermal conductivity and mass diffusion can take the following forms respectively:

$$k = \frac{\mu \, c_p}{p_r}, \qquad D = \frac{\mu}{\rho \, Sc} \tag{18}$$

Where Pr and Sc are Prandtl and Schmidt numbers respectively and there value are considered constant.

The rate of droplet radius R change is given by Frossling correlation [9],

$$R = -\frac{(\rho D)_{air}(\hat{T})}{2\rho_d r}\frac{Y_1^* - Y_1}{1 - Y_1^*} Sh_d, \tag{19}$$

Where Sh is the Sherwood number for mass transfer, Y_1^* is the water vapor mass fraction at the droplet's surface, $Y_1 = \rho_1 / \rho$, and $(\rho D)_{air}(\hat{T})$ is the water vapor diffusivity in air. The Sherwood number is given by

$$Sh_d = (2.0 + 0.6\,\mathrm{Re}_d^{\frac{1}{2}} Sc_d^{\frac{1}{3}})\frac{\ln(1 + B_d)}{B_d}, \tag{20}$$

Where

$$Sc_d = \frac{\mu_{air}(\hat{T})}{(\rho D)_{air}(\hat{T})}, \qquad B_d = \frac{Y_1^* - Y_1}{1 - Y_1^*} \tag{21}$$

The surface mass fraction Y_1^* is obtained from

$$Y_1^* = \frac{W_1}{W_1 + W_0\left(\frac{p}{p_0(T_d)} - 1\right)} \tag{22}$$

Where W_0 is the local average molecular weight of the dry air and $p_0(T_d)$ is the equilibrium water vapor pressure at the droplet temperature.

Droplet Energy Equation

The rate of droplet temperature change $T_d^{\bullet}$ is determined by energy balance:

$$\rho_d \frac{4}{3}\pi r^3 c_l T_d - \rho_d 4\pi r^2 R L(T_d) = 4\pi r^2 Q_d \tag{23}$$

Where c_l is the liquid specific heat, $L(T_d)$ is the latent heat of vaporization. R is the rate of droplet radius change, which is given by Frossling correlation $R = -\frac{(\rho D)_{air}(\hat{T})}{2\rho_d r}\frac{Y_l^* - Y_l}{1 - Y_l^*} Sh_d$. Q_d is the rate of heat conduction to the droplet surface per unit area. $Q_d = \frac{K_{air}(\hat{T})(T - T_d)}{2r} Nu_d$ Both Sherwood (*Sh*) and Nusselt (Nu) numbers can be calculated according to the modified Ranz-Marshall correlations [9] which takes the following forms:

$$Sh_d = (2.0 + 0.6\,\mathrm{Re}_d^{\frac{1}{2}} Sc_d^{\frac{1}{3}})\frac{\ln(1 + B_d)}{B_d}, \quad Nu_d = (2.0 + 0.6\,\mathrm{Re}_d^{\frac{1}{2}} \mathrm{Pr}_d^{\frac{1}{3}})\frac{\ln(1 + B_d)}{B_d}$$

Where $B_d = \frac{Y_l^* - Y_l}{1 - Y_l^*}$ and Y_l^* and Y_l are the droplet surface and the surrounding mass fractions respectively, while the temperature $\hat{T} = (T + 2\,T_d)/3$

Other sub-models have been used. These sub-models are those of turbulent dispersion of droplets, droplets breakup and collision models. The models used in KIVA III code for droplets turbulent dispersion and breakup (TAB model), have been used in this simulation without modifications. Regarding the droplet collision model, the collision frequency has been modified [10] to improve the prediction accuracy as follows:

$$\nu = \frac{N_2}{V_{ijk}}\pi\left(r_{p1} + r_{p2}\right)^2 \frac{\left(\left(\vec{V}_1 - \vec{V}_2\right) \bullet \left(\vec{X}_2 - \vec{X}_1\right)\right)}{\left|\vec{X}_2 - \vec{X}_1\right|} \tag{24}$$

Where X1 and X2 are the physical locations of droplets 1 and 2 respectively in the collision volume.

SOLUTION ALGORITHM

It is clear that, the physical model is too large to be simulated numerically with reasonable accuracy. As shown in Fig. 2, the nozzles matrix is constructed of repeated similar parts, each of which is bounded by planes of symmetry at the four faces parallel to the main airflow direction. Any of these parts could be the domain of study. However, the nozzles lay next to the walls cannot be simulated by the aforementioned domain because of the deviation from symmetry due to the effect of wall boundary layer. For these cases representative domains are considered to take into account the wall effect. For the nozzles near the wall, they can be classified into two cases. The first is a nozzle, which has a wall at one side and the other three sides are occupied by another nozzles. The second is a

nozzle, which lies at a corner of the duct. In this case it will have two walls that form the corner and two sides which are occupied by other nozzles. The first case, as shown in Fig. 3, is designated as the side wall case. For this the computational domain will extend from the wall to the symmetry plan between the second and the third nozzle from the wall at which the wall effect on symmetry is diminished. Regarding the corner case the domain of study is shown in Fig.3. Other corners will have a similar domain with consideration of the direction of the corner's rigid walls.

According to this, three types of solution domains are identified. These include the main stream, the side wall and the corner domains. The complete solution for the cross section is the assembly of the suitable domains to represent the whole cross section.

Regardless this manipulation for the cross section, the length in the flow direction (i.e. 6m) is still too large to be simulated with reasonable accuracy. A numerical technique which benefits from the hypothesis that the flow has a parabolic nature is considered. This technique is also based on the assumption that the pressure along the domain remains constant. The technique includes dividing the domain along the flow direction into a number of parts (blocks), as shown in Fig. 4. These blocks are simulated consecutively in series from upstream to downstream. The flow in each block is simulated until steady state condition is reached. The un-change of the average air temperature over a definite period of time is taken as a sign for reaching the steady state flow. The outlet conditions for the steady state condition of a block are taken to be the inlet boundary conditions to the next block. The initial conditions of this new block are considered to be the same as the steady state flow conditions of the previous block. At the transition from one block to the next, the properties of the cells in the last plan of the block are taken as the inlet boundary conditions of the new block. If the positions of the grid's cells are changed, the values of the boundary conditions are interpolated for the new grid. This option gives the ability of changing the cell sizes as the simulation process marches downstream. The properties, which are taken into consideration at the interface between the blocks, are air velocities, species concentration, turbulent kinetic energy and its dissipation. The inlet pressure is assumed constant. The inlet temperature of the gas mixture is calculated by using the ideal gas relation from the known inlet species concentrations and the inlet pressure.

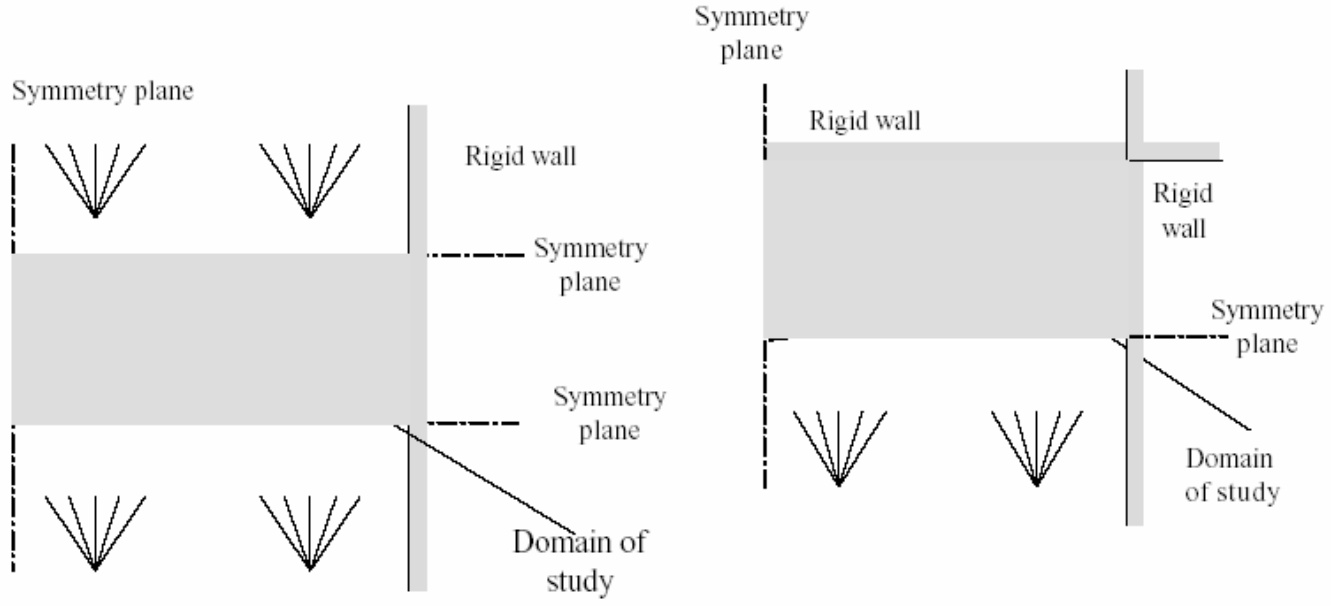

Fig.3 The side and corner solution domains

The transmission of the droplets from one block to another is the most sophisticated process in this technique. Two approaches have been tried. The first is the storage of the parcels properties at the exit of the block over a certain time. The storage begins after the steady state condition is achieved. The time delay at which the parcels exit from the block after the beginning of the storage process is calculated. The storage parcels are re-injected in the next block over repeated cycles of time as same as the storage period. In each cycle the parcels are injected at its time delay from the beginning of the cycle. The main drawback of this approach is a noticeable fluctuation in the ratio of the total water (liquid and vapor) to the air. These fluctuations is accumulated to produce after approximately thirty block an error of 6% in the ratio of total liquid to air.

The second approach differs from the first in the re-injection technique of the parcels. The parcels are re-injected in the same order of their exit with a constant rate. This rate is calculated by subtracting the amount of water vapor in the air flow from the inlet total amount of water. This condition permits the conservation of constant total water flow rate. Another condition is considered to permit the conservation of constant dry air during the transmission from block to another. The parcels properties, which are taken into consideration during the transmission process, are the parcel physical coordinates x, y and z, mean velocities and turbulent velocities, the droplet radius and temperature, the number of droplets per the parcel, and the oscillation parameters considered by the breakup model. This technique has the advantages of high solution stability as well as accuracy. Therefore, this technique has been adopted. In this respect it is important to mention that the consecutive block technique improved the efficiency of the solution tremendously. Full solution can be achieved with the use of five centimeters block at a time order of $(1/120)^2$ compared with the normal technique of simulating the whole system with one block.

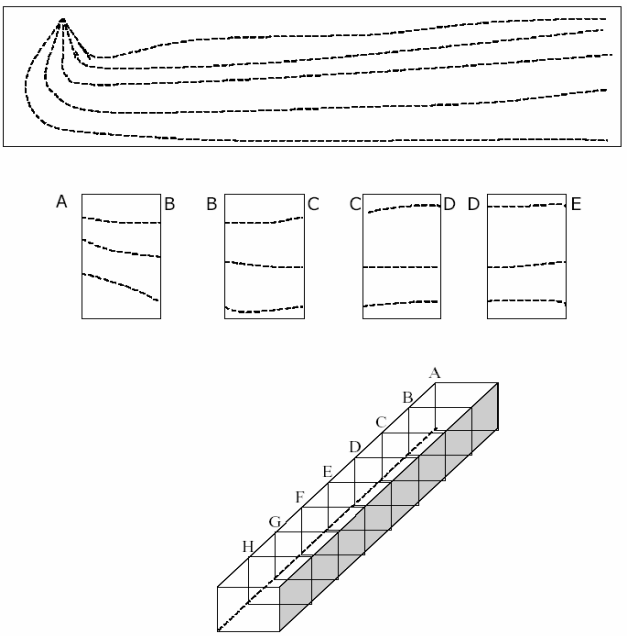

Fig. 4 Schematic diagram of the consecutive block technique concept

Regarding the boundary conditions, the symmetry planes have zero tangential shear stress and its normal air velocity equals zero. For the rigid wall, the law of wall is applied. Regarding thermal boundary conditions, the wall is considered to be adiabatic. For the inflow boundary, it has a constant velocity with only an axial component perpendicular to the inlet plane and the other components are set to zero. The inlet species density are taken to be as that of the air at the implemented conditions. The pressure is determined from the domain calculation while the temperature is calculated from the ideal gas relations. Regarding the outflow boundary, the velocity components at the boundary vertices are set equal to those of the logical inside neighboring vertices. The outlet pressure is set to 1.03 bar, which is specified at a distance equal to one centimeter outside the boundary. This is important to prevent the reflection of the acoustic wave which can affect the upstream flow.

Regarding the spray, the injected droplets sizes are chosen stochastically according the following distribution.

$$g(r) = \frac{r^3}{6\bar{r}^4} e^{-\frac{r}{\bar{r}}} \tag{25}$$

Where $\bar{r}$ is the number average drop radius, which for the above distribution is related to the injected Sauter mean radius.

$$\bar{r} = \frac{1}{3} r_{32} \tag{26}$$

The droplets size is then chosen randomly by comparing the inverse of the cumulative function of the above distribution with a random number uniformly distributed between 0 and 1. The inversion of the cumulative function is performed numerically in step of 0.12 $\bar{r}$. The value of this inversion is taken to be unity at r = 12 $\bar{r}$. The conditions implemented on the droplets when they cross any of the boundaries are as follow. For rigid wall, the droplets are excluded from the calculations without being removed from the domain. For the symmetry plan, the droplets are reflected into the domain as a mirror image. For the input and output faces, the droplets are removed from the domain.

Regarding the gas initial conditions they are taken to be uniform over the domain with the same inlet condition of the gas. This hypothesis is acceptable because it assumes that the injection start after the beginning of simulation. The pressure value is taken to be the value of standard atmospheric pressure at the sea level.

RESULTS

Considering the physical model, certain configuration was chosen to represent a base case. In this base case, water is injected in a perpendicular direction to the main airflow direction (cross-flow). The injector type is considered to be a high-pressure atomizer that produces a full cone spray. Injected water temperature equals to the wet bulb temperature of the inlet air. Both the properties as well as conditions of the inlet airflow are considered to be homogenous. The quantity of injected water is defined based on the inlet and targeted (at the outlet) humidity, as follows:

$$m^{\bullet}_{inject} = (\psi_{out} - \psi_{in}) \times \rho_{air} \times V_{air} \times A \tag{27}$$

Where V_{air} is the inlet air velocity, and "A"is the cross sectional area of the studied domain. Table 2 summarizes the values of the parameters considered in the base case.

Spray dispersion into the air is the controlling factor of humidification. Achieving homogeneous droplets distribution over the airflow cross section ensures homogenous as well as efficient humidification. Figure 5 shows the spray configuration over 30 cm from the entrance section and under the effect of the cross flow. From the figure it can be noticed that, the spray cone angle has been decreased to 60^o instead of 70^o. A zone of high droplets concentration exists at the bottom of the spray after it yields in the direction of the main air stream. This is attributed to the nature of the spray as a solid cone with high concentration at the spray axis. Due to the combined effect of spray penetration and yielding with the air flow, the spray axis becomes more close to the bottom surface of the duct and thus high concentration is found in this zone. At the first ten centimeters the rate of spray penetration decreases as the droplets yield in the direction of the main air stream. After these ten centimeters the rate of penetration remains almost constant. This can be explained in the light of high momentum transfer between the droplets and the air during the first stage. As the droplets loose their momentum and yield in the direction of airflow, they move with the air with almost no slip.

Table (2) Values of the parameters considered for the base case

Parameter	Base case Value
Inlet air velocity	2 m/s
Inlet air turbulent Kinetic energy	5 % of total Air K.E.
Inlet air temperature	40^o C
Inlet relative humidity	40 %
Initial droplet SMD	25 μm
Initial droplet velocity	20 m/s
Initial droplet temperature	27.82^o C
Spray cone angle	70^o
Rate of water injected per nozzle	0.53 gm/sec
Orientation of injection direction relative to air stream	90^o

Figure 6 shows the droplets distribution at different axial distance ranges along the duct. At the first section, which represents the injection section, the cone angle from this view is 70^o as indicated in the injection parameters. The droplets concentration is the highest at the spray centerline. At this section the spray covered area represents only 25% of the duct area. Moving with the spray along the duct, the spray impinges the opposite spray at a distance 55-60 cm from the entrance. As a result of the opposite sprays impingement the spray changes its direction and move to the sides such that it reaches the side symmetry planes which separate the two adjacent sprays. At this section it can be observed that most of the droplets are concentrated near the symmetry planes. At about two meters from the entrance the spray approximately covers all the area of the duct section, except an area around the water feeder. However the distribution is not homogeneous. Moving with the duct and due to the air secondary motion the droplets move downward to fill the center of the cross section. This improves droplets distribution over the duct cross section.

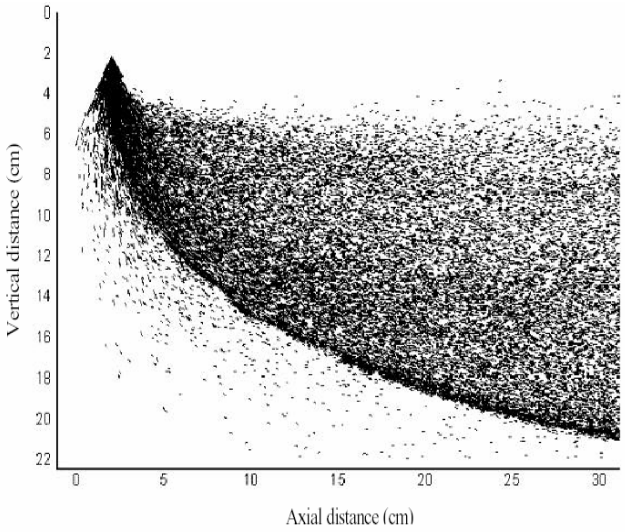

Fig. 5 Spray Behavior in the First 30 cm for the Injection Section

Accordingly, the main mechanism of the droplets dispersion is the secondary flow as well as the vortices initiated due to the cross injection of the water into the air. The full cone configuration and the concentration of the maximum flow rate at the spray axis causes inefficient dispersion at the beginning. Lack of good dispersion in the beginning prevents homogeneous droplets distribution in the successive sections.

Figure 7 shows the air relative humidity at different cross sections along the duct. Comparing this Figure with Fig. 6, it can be found that, the areas where the relative humidity increases are those occupied by water droplets. Accordingly, relative humidity distributions are very similar to that of the droplets. However the highest value of the relative humidity is located at the center of the two vortices created due to the impingement of the two opposing sprays, which is not the location of maximum droplets mass flow rate. This difference is attributed to the fact that the relative humidity increase is due to the cumulative evaporation over the previous sections. The second reason is that water evaporates faster at the higher turbulent intensity zones, where this condition is maximum at the vortices centers. Moving along the duct, it can be noticed that the same pattern is prevailing. As a summery, the history of the evaporation process is very effective on the final relative humidity distribution. This means that initial droplets dispersion affects the final relative humidity distribution and value. These highlight the importance of the initial dispersion of the water droplets and consequently spray injection characteristics.

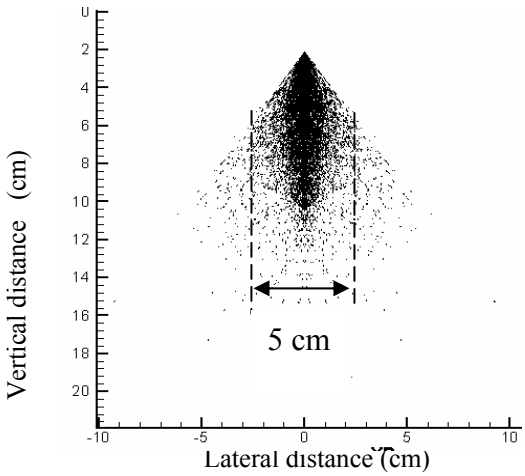

a) At range of 0-5 cm from nozzle

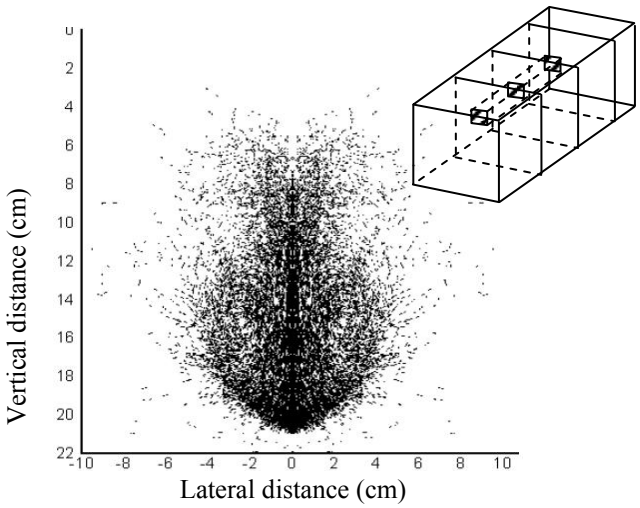

b) At range of 25-30 cm from nozzle

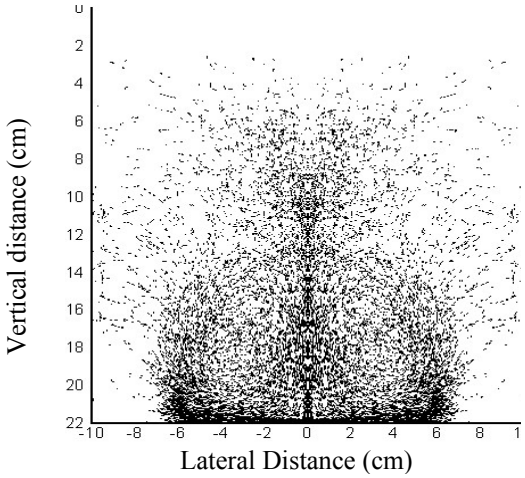

c) At range of 55-60 cm from nozzle

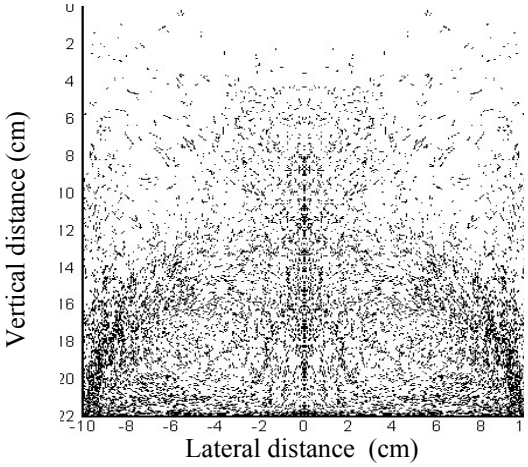

d) At range of 95-100 cm from nozzle

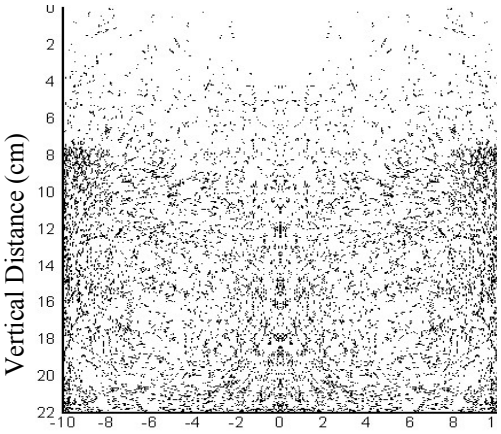

e) At range of 195-200 cm from nozzle

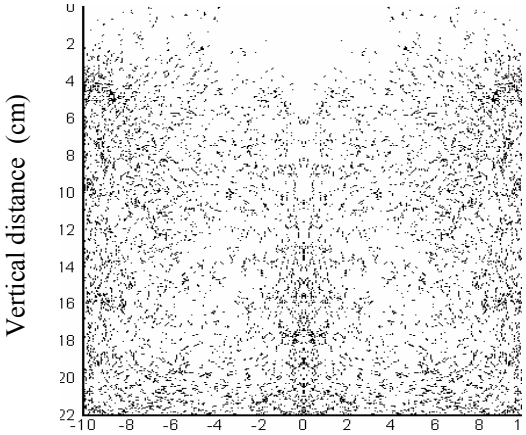

f) At range of 295-300 cm from nozzle

Fig. 6 Droplet Distribution Along the Duct

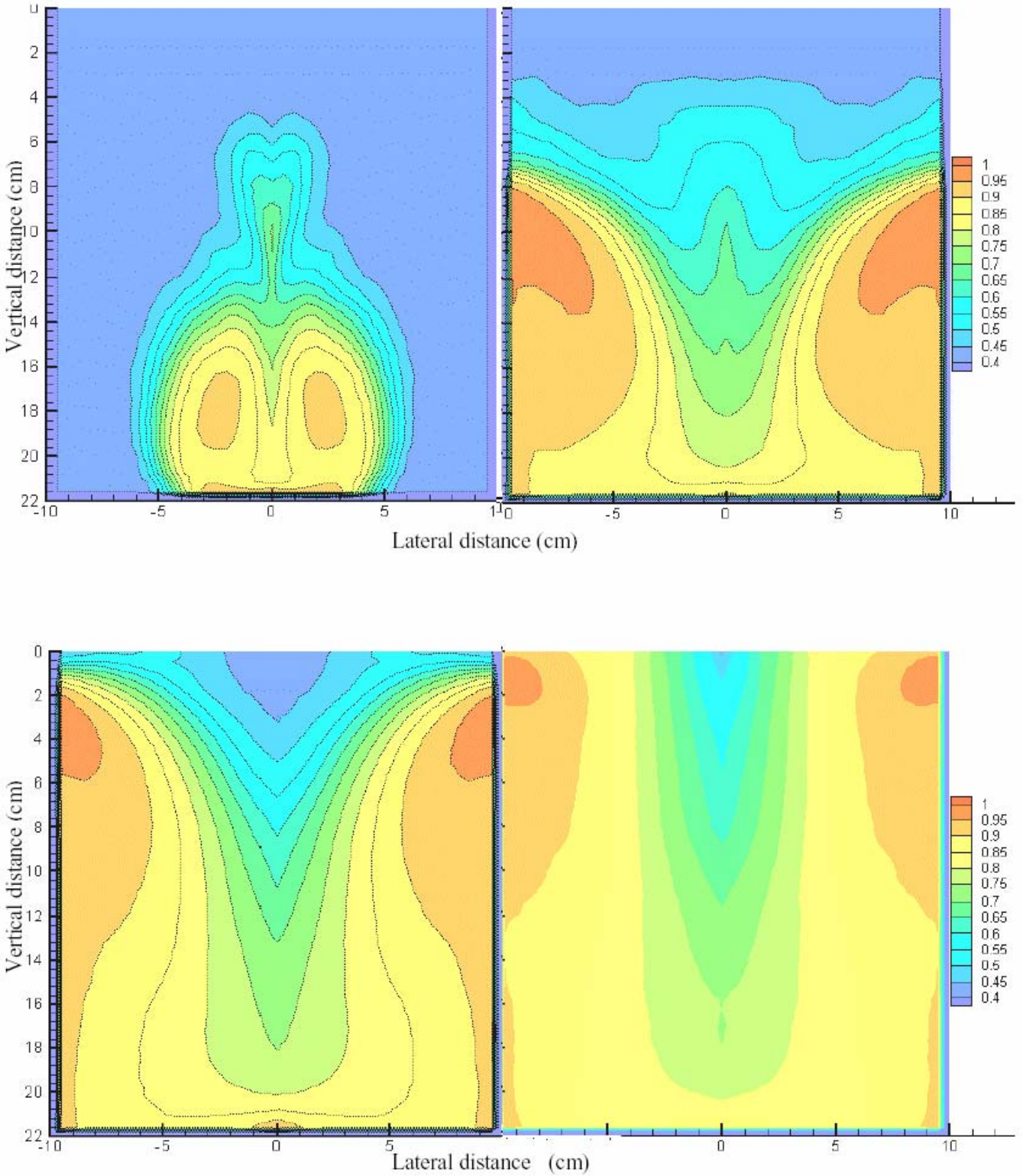

Fig. 7 Contours of Relative Humidity at Different Sections along the Duct

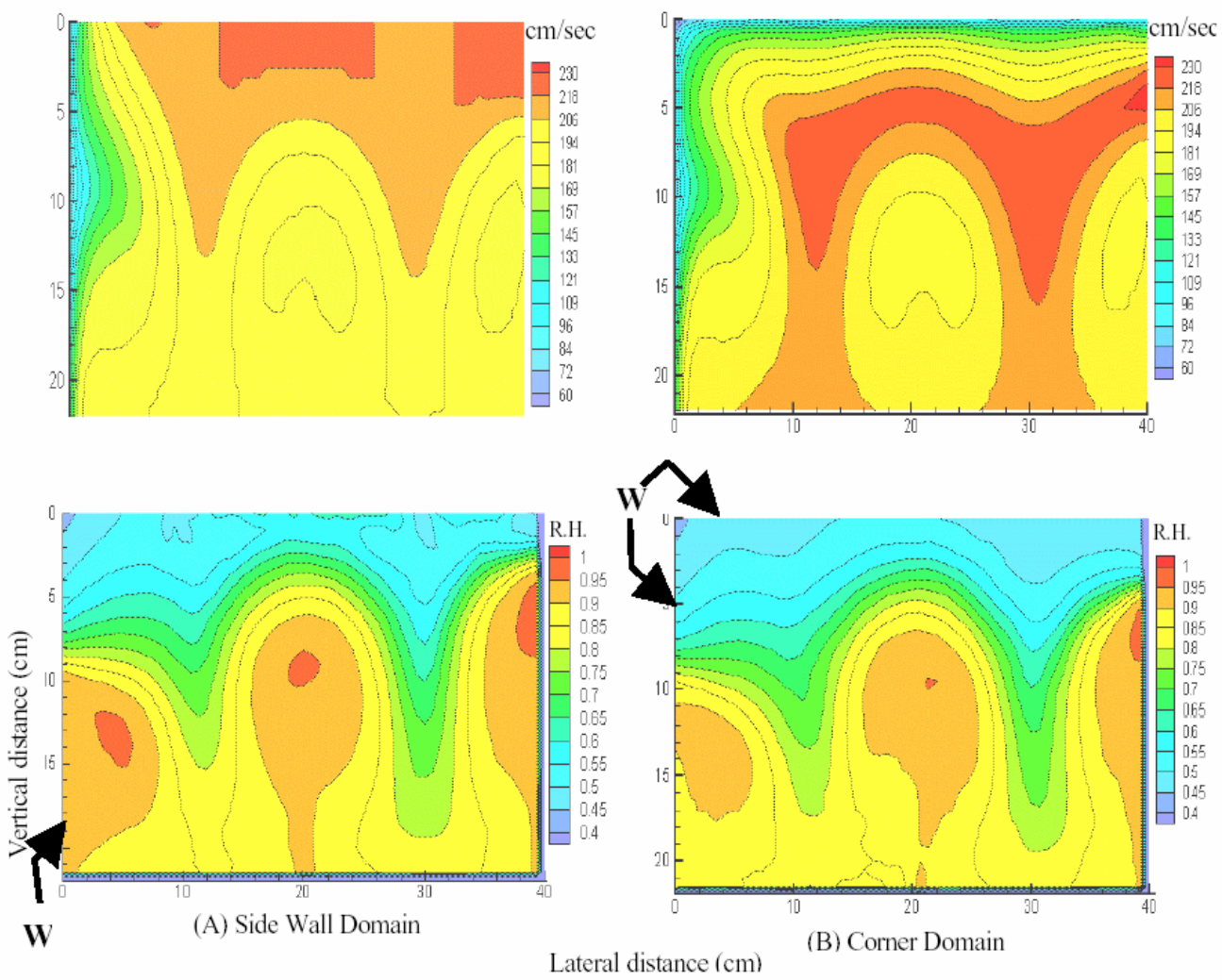

Fig. 8 Contours of Main Stream Air Veloity and Relative Humidity at the Wall and Corner Domains

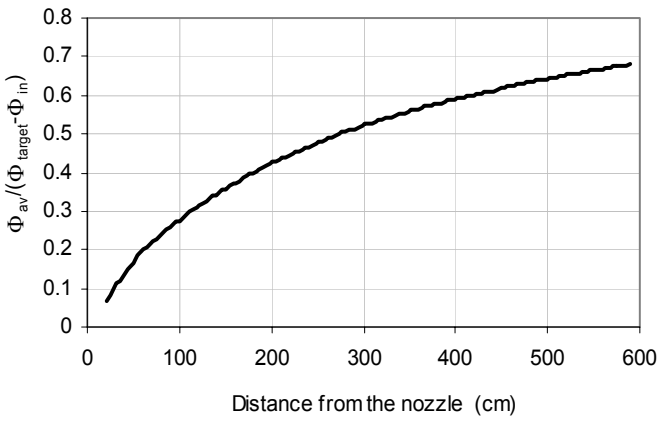

Fig. 9 Evolution of the relative humidity along the duct

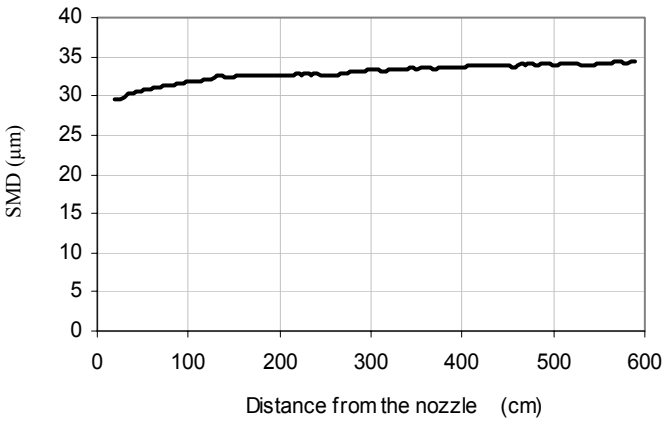

Fig. 10 Change in the droplets Sauter mean Diameter (SMD) along the duct

Regarding the region close to the duct walls as well as corners, Fig.8a shows the humidity contours at these regions at a section 4 m from the injection section. The wall effect in this section appears clearly. The rigid wall prevents the air and the droplets to move upward as in case of the other side of the domain. This leads to the circulation of the droplets in the bottom left corner of the domain. Thus the relative humidity in this section increases. This behavior leads to a poor humidity distribution near the wall and less quantity of the evaporated water. The other observation is the rapid propagation of the droplets as we move away from the side wall. This leads to enhance the propagation of the relative humidity near the symmetry plane.

Regarding the region at the duct corner and at a distance 4 m downstream the injection plane, the effects of the two rigid walls appear clearly, as shown in Fig. 8b. The first effect is that the area of high relative humidity is pushed down from the upper wall due to the gross of the boundary layer. The second effect is the general decrease in the relative humidity compared with that far from the wall. This is especially noticed at the areas that have relatively high relative humidity.

Regarding the development along the duct, Figure 9 and 10 show the changes in the dimensionless parameters for humidity and droplet Sauter mean diameter along the duct respectively.

Regarding the effect of different parameters on humidifaction process, four design and operational paramters have been investigated. The design paramters are; injected Sauter mean diameter of the droplets, intial turbulent kinetic energy of the airflow and orientation angle between injected liquid and airflow. The operational parameters are represented by initial relative humidity. Figure 11-14 show the effect of these paramters on humidifaction process as well as its homogenity. Humedification improvement is represented by the average relative humidity of the exit section of the duct divided by the corresponding value of the base case. Humidification homogenity is evaluated by the standard deviation of the relative humidity over the last section of the duct. As the value of the standard deviation increases this means higher variation in the relative humidity over the section.

From these figures it can be concluded that inlet turbulent kimetic energy has a minor effect on the average value of the relative humidity at the end section of the duct. However it improves the homogenity of the relative humidity over that section. Regarding the injected Sauter mean diameter, it improves the humidifiaction process at the duct as the injected droplets diameters become less. On the other hand it has a minor effect on the homogenity of the relative humidity over the end section. The change in the average droplet size at the end section of the duct represents a linear relation between the inlet droplet size and the exist one, as shown in Fig. 15. This result is very important for the studies of the inlet duct cooling in the gas turbine.

Regarding the orientation angle the cross injection orientation has the highest humidification effectiveness, while the counter flow orientation has the best homogenity for the relative humidity over the the end section.

Finally regarding the change in the initial relative humidity, best conditions regarding the system effectiveness and homogenity is found at low inlet relative humidity.

CONCLUSIONS

Humidification process of airflow through a rectangular duct utilizing a matrix of injection nozzles has been simulated numerically. The simulation is three dimensional, turbulent with consideration of full coupling between the droplets and airflow. The large system size which could make numerical simulation forbiden has been overcome through dividing the cross section into symmetical moduls with special moduls for the side and corner cases. On the other hand the consecutive block technique represented a powerful tool in simulating the large system size along its axis as well as offered better computational efficiency. The results of simulation showed the dependency of humidifcation efficiency on the droplet dispersion, especially at the first part of the duct. The parametric study showed that the cross flow injection is the most effective orientation regarding humidification efficincy compared with the counter flow orientation which offers the best humidity homgenity. The decrease in the injected droplet size improves humitification. Furthermore exit droplet size scales linearly with the injected one. Finally the inlet turbulent kinetic energy has a minor effect on humidifaction efficiency, however it improves its homogenity.

REFERENCES

1. El-Salmawy H., and Gobran M.”Impacts of Controlling Inlet Conditions to Gas Turbine Based Power Plants”, ISABE-2005-1211, Munich, 2005
2. Ghosh S. and Hunt, J.C.R.,” Spray Jets in a Cross-Flow”, Journal of Fluid Mechanics, Vol, 365,pp. 10-136, 1998.
3. Mashayek, F., Jaberi, F.A., Miller, R.S., Givi, P., “Dispersion and Polydispersity of Droplets in Stationary Isotropic Turbulence”, Int. J. Multiphase Flow, 23 (2), 337-335, 1997.
4. Mashayek, F.,”Direct Numerical Simulations of Evaporative Droplet Dispersion in Forced Low Mach Number Turbulenc”, Int.J. Heat and Mass Transfer 41(7), 2601-2617, 1998-a.
5. Crowe, C.T., Sharma, M.P., and Stock, D.E., “The Particle-Source-In-Cell Method for Gas Droplet Flow”, J. Fluid Engr., 99, 325, 1977.
6. Kahhwaha, S.S., Dhar, P.L., and Kale, S.R., “Experimental Studies and Numerical Simulation of Evaporative Cooling of Air with Water Spray-I. Horizontal Parallel Flow”, Int. J Heat and Mass Transfer, Vol. 41, No. 2, pp 447-464, 1998-a.

7. Kahhwaha, S.S., Dhar, P.L., and Kale, S.R., "Experimental Studies and Numerical Simulation of Evaporative Cooling of Air with Water Spray-II. Horizontal Counter Flow", Int. J Heat and Mass Transfer, Vol. 41, No. 2, pp 465-474, 1998-b.
8. Sanjeev Jolly, P.E., Joseph Nitzken, P.E. and Donald Shapherd, "Capacity Enhancement of ABB 11N1 with thermal Energy Storage", The Power-Gen International, New Orliens, Louisiana, 1999.
9. Amsden, A.A., O'Rourke, P.J., Butler, T.D., "KIVA-II: A Computer Program for Chemically Reactive Flows with Sprays", Los Alamos National Laboratory Report LA-11560-MS, UC-96, May 1989.
10. 10.Awny, K. M., "Numerical Simulation of Air Humidifaction Process Using Modified Droplets Collision Model" M.Sc., Cairo University, 2003.

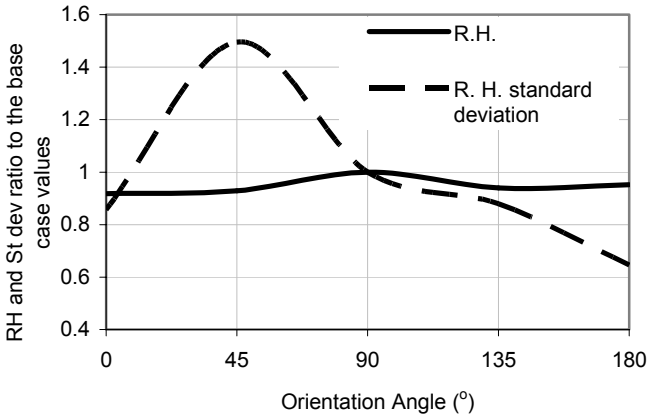

Fig. 13 Effect of Orientation Angle between Injection and Airflow on the Relative Humidity and its Homogeneity at the Exist Section of the Duct

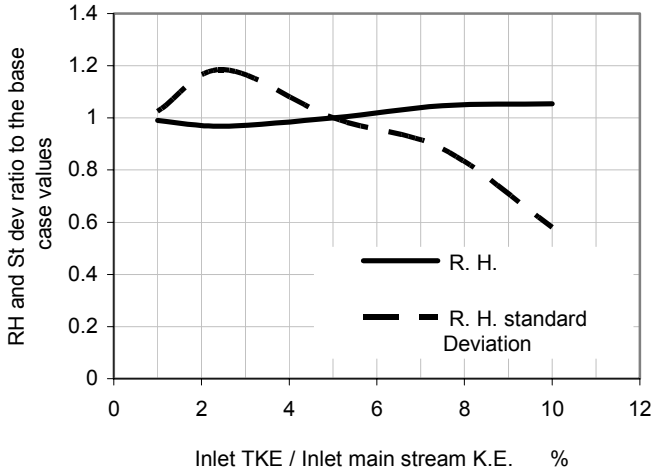

Fig. 11 Effect of Inlet Turbulent Kinetic Energy on the Relative Humidity and its Homogeneity at the Exist Section of the Duct

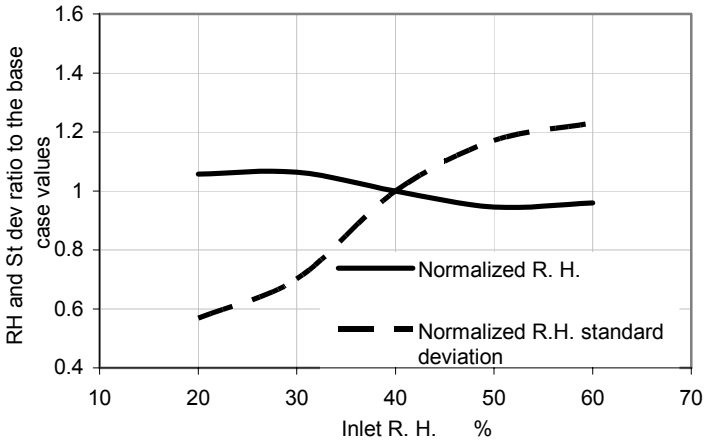

Fig. 14 Effect of Inlet Relative Humidity on the Relative Humidity and its Homogeneity at the Exist Section of the Duct

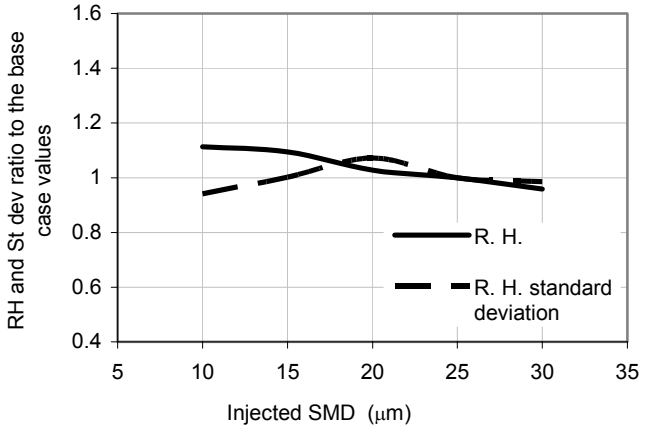

Fig. 12 Effect of Sauter Mean Diameter on the Relative Humidity and its Homogeneity at the Exist Section of the Duct

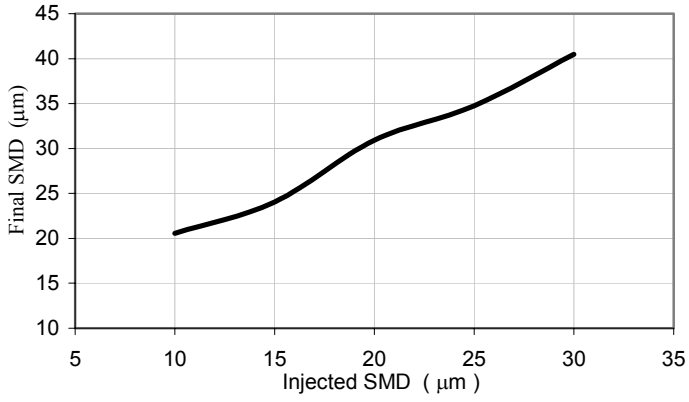

Fig. 15 Effect of the Intial Sauter Mean Diameter of the the Average Droplet Size over the Exist section of the Duct